

Cite this: *Phys. Chem. Chem. Phys.*, 2011, **13**, 3775–3781

www.rsc.org/pccp

PAPER

## Macromolecular dynamics of conjugated polymer in donor–acceptor blends with charge transfer complex†

Olga D. Parashchuk,<sup>ab</sup> Tatyana V. Laptinskaya<sup>a</sup> and Dmitry Yu. Paraschuk<sup>\*ab</sup>

Received 4th September 2010, Accepted 11th November 2010

DOI: 10.1039/c0cp01710h

Donor–acceptor blends based on conjugated polymers are the heart of state-of-the-art polymer solar cells, and the control of the blend morphology is crucial for their efficiency. As the film morphology can inherit the polymer conformational state from solution, the approaches for probing and controlling the polymer conformational state in the blends are of high importance. In this study, we show that the macromolecular dynamics in solutions of the archetypical conjugated polymer, MEH-PPV, is essentially changed upon addition of an acceptor 2,4,7-trinitrofluorenone (TNF) by using dynamic light scattering (DLS). We have observed four new types of the macromolecular dynamics absent in the parent polymer determined by the polymer and acceptor content. The MEH-PPV : TNF ground-state charge-transfer complex (CTC) is suggested to result in these dynamics. In the dilute polymer solution, the CTC formation leads to slower dynamics as compared with the pristine polymer. This is evidence of aggregates formed by intercoil links that are the CTCs involving two conjugated segments of different coils with acceptor molecules being sandwiched between them. At low acceptor content, the aggregates are not stable but at high acceptor content, they are. In the semidilute solution at low acceptor content, the dynamics becomes faster as compared with the pristine polymer that is explained by confinement of the coupled motions of entangled polymer chains. At high acceptor content, the dynamics is far much slower with a characteristic long-range correlation at the scale 3–5  $\mu\text{m}$  that is explained by aggregation of polymer chains in clusters. One can expect that the DLS technique could become a useful tool to study the nano- and microstructure of donor–acceptor conjugated polymer blends to achieve controllable morphology in the corresponding blend films.

### Introduction

Blends of conjugated polymers with organic acceptors are actively studied as promising materials for organic solar cells and photodetectors. The semiconducting properties of conjugated polymers strongly depend on their conformational state as they are closely related to the degree of  $\pi$ -electron delocalization along the conjugated segments. Moreover, the polymer conformational state can be inherited from solution into film<sup>1</sup> that could be used to control the film morphology and therefore its semiconducting properties, *e.g.* the charge mobility. Accordingly, a study of the macromolecular dynamics of conjugated polymers in solution can be used as a means to address the relation between the polymer conformational state

in solution and film morphology. It was recently found that conjugated polymers can form weak intermolecular ground-state charge-transfer complexes (CTC) in blends with organic acceptors.<sup>2–6</sup> On the one hand, the CTCs have attracted significant attention as an important intermediate on the way from excitons to free charges in organic solar cells,<sup>7–9</sup> especially in polymer–fullerene ones.<sup>10–12</sup> On the other hand, the CTC can influence the donor–acceptor phase separation in the blend films<sup>13</sup> and hence change the blend morphology. The latter is of paramount importance for efficient bulk-heterojunction solar cells.<sup>14</sup> Moreover, the very recent studies suggest that the CTC formation can change the polymer conformational state in the blend.<sup>15,16</sup> One could expect that the conformational changes in the solution of conjugated polymer resulting from the CTC formation can be probed by dynamic light scattering (DLS) that could give information about molecular conformational state.

The DLS technique is routinely used to investigate the macromolecular dynamics in solution. The autocorrelation function (ACF) of light scattered by concentration fluctuations is measured, and it gives the relaxation times of

<sup>a</sup> Faculty of Physics, M.V. Lomonosov Moscow State University, Moscow 119991, Russia

<sup>b</sup> International Laser Center, M.V. Lomonosov Moscow State University, Moscow 119991, Russia. E-mail: paras@physics.msu.ru

† Electronic supplementary information (ESI) available: The ACFs and the corresponding RTDs for MEH-PPV : TNF = 1 : 0.5 dilute blend and pristine MEH-PPV solutions for various concentration. See DOI: 10.1039/c0cp01710h

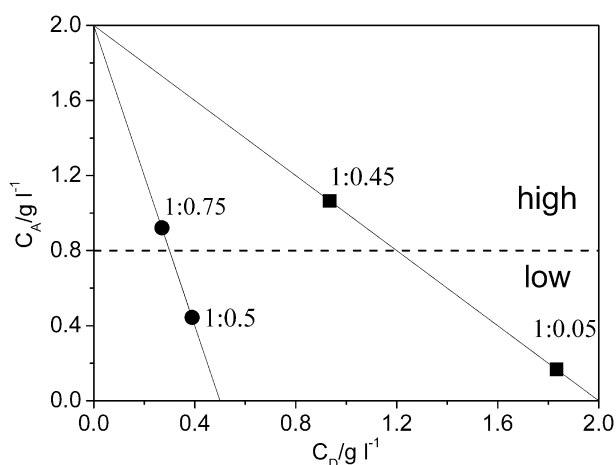


**Fig. 1** The donor and acceptor concentrations in MEH-PPV:TNF blends for different initial concentrations ( $C_D^0 = C_A^0 = 2 \text{ g l}^{-1}$  – squares and  $C_D^0 = 0.5 \text{ g l}^{-1}$ ,  $C_A^0 = 2 \text{ g l}^{-1}$  – circles). The dashed line separates the ranges of low and high acceptor content.

characteristic motions of the light scatterers. The type of macromolecular motion, *e.g.*, diffusion, can be identified from the relaxation time dependence on the scattering vector  $q = (4\pi n/\lambda)\sin \theta/2$ , where  $n$  is the refractive index of a solvent,  $\lambda$  is the excitation wavelength, and  $\theta$  is the scattering angle. The type of dynamics could give information about the conformational state of molecules, *e.g.*, for diffusion dynamics the hydrodynamic radius can be calculated by using the Einstein–Stokes relationship:

$$R_h = \frac{kT}{6\pi\eta_0 D}, \quad (1)$$

where  $k$  is the Boltzmann constant,  $T$  is the temperature,  $\eta_0$  is the solvent viscosity, and  $D$  is the diffusivity. Eqn (1) gives the macromolecule hydrodynamic radius for dilute solution and the correlation length  $\xi$  for semidilute one.<sup>17</sup> The correlation length is the distance at which the concentration fluctuations are correlated.

The dynamics of conjugated polymers was earlier studied by DLS: the hydrodynamic radius was determined in different

solvents in dilute solution,<sup>18–20</sup> the aggregate and polymer network formation in PPV-derivatives were observed in semidilute solution<sup>20–22</sup> and assigned to  $\pi$ – $\pi$  interaction between the polymer chains.<sup>20,22</sup> Moreover, the conformational state of one of the most studied conjugated polymer poly(methoxy,5-(2'-ethyl-hexyloxy-1,4-phenylene-vinylene)) (MEH-PPV) was studied by small-angle neutron scattering, and MEH-PPV was shown to form disk-like aggregates in toluene.<sup>23</sup> However, the dynamics and conformational state of conjugated polymers in donor–acceptor blends have not been studied so far. As shown below, we do not observe aggregates in the pristine MEH-PPV chlorobenzene solution that would be related to  $\pi$ – $\pi$  stacking; however, aggregates and clusters are found to be formed upon acceptor addition both in dilute and semidilute donor–acceptor blends, correspondingly.

In this paper, we show that the CTC formation results in different macromolecular dynamics in donor–acceptor blends which qualitatively changes with polymer concentration and polymer:acceptor ratio (acceptor content). We study donor–acceptor blends of MEH-PPV and low-molecular-weight organic acceptor 2,4,7-trinitrofluorenone (TNF) in which a pronounced Mulliken-type ground-state CTC was found to be formed.<sup>2–4</sup> We observe four types of macromolecular dynamics in the blend, *i.e.*, in dilute/semidilute solution at low/high acceptor content, that are distinct from those of the pristine polymer and explain them by CTC properties.

## Experimental

DLS studies were conducted with the use of a correlator-goniometer ALV-CGS-5000/6010 (Langen, Germany) equipped with a He-Ne laser radiating with a wavelength of 633 nm, the power at the sample was 20 mW, and the light intensity was  $115 \text{ W cm}^{-2}$ . We will refer to the power as 100%. The optical length of the cuvette was 0.8 cm. The ACF of light scattered by concentration fluctuations in the sample was measured at 100% power if not mentioned otherwise. To obtain the relaxation time distributions, the ACFs were processed by the software “CONTIN” employing inverse Laplace transformation. A relaxation time distribution can be recalculated into an apparent hydrodynamic radius or correlation length

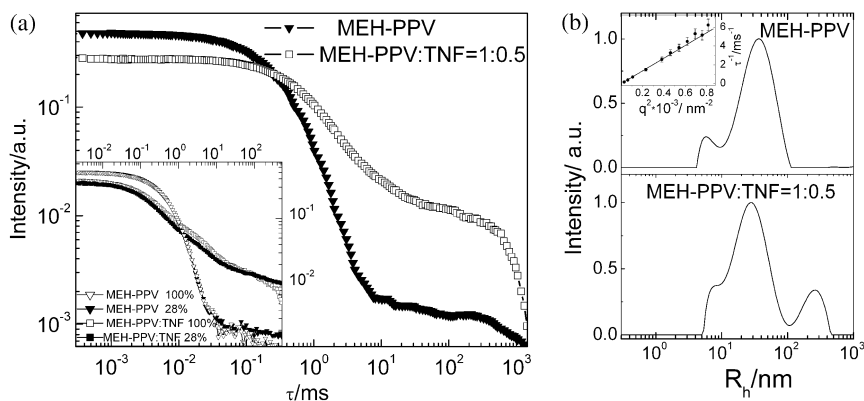


**Fig. 2** Dilute solution data: (a) ACFs and (b) the corresponding HRDs for dilute  $0.5 \text{ g l}^{-1}$  pristine MEH-PPV (full triangles) and for MEH-PPV:TNF = 1:0.5 (open squares) blend, the scattering vector  $q = 0.01 \text{ nm}^{-1}$  ( $\theta = 40^\circ$ ). The inset in panel (a) shows the ACFs for different laser powers used for recording the DLS data. The inset in panel (b) shows the inverse relaxation time  $\tau^{-1}$  for dilute MEH-PPV *vs.*  $q$ , the line is a linear fit  $\tau^{-1} = Dq^2$  with  $D = (6.8 \pm 0.3) \times 10^{-8} \text{ cm}^2 \text{ s}^{-1}$ .

distribution (HRD or CLD) by using the Stokes–Einstein relation (eqn (1)) with  $\eta_0 = 0.8$  cP for chlorobenzene.

TNF and MEH-PPV (Sigma-Aldrich,  $M_n = 86\,000$ ,  $M_w = 420\,000$ ) were dissolved separately in chlorobenzene at initial concentrations  $C_A^0 = 2\text{ g l}^{-1}$  and  $C_D^0 = 0.5\text{ g l}^{-1}$  and  $2\text{ g l}^{-1}$ , correspondingly. The solutions of MEH-PPV ( $C_D^0 = 0.5\text{ g l}^{-1}$ ) and TNF were filtered using PTFE filters (Millex 0.45  $\mu\text{m}$ ) and then mixed at acceptor content  $x = C_A/(C_A + C_D)$ , where  $C_A$  and  $C_D$  are the acceptor and donor concentrations in the blend, respectively. The acceptor content is referred to as MEH-PPV:TNF = 1 :  $x$ . The  $C_A$  and  $C_D$  used are shown in Fig. 1 as the ( $C_A$ ,  $C_D$ ) plot.

## Results and discussion

First of all, the overlap concentration in MEH-PPV solution was found to be about  $1.5\text{ g l}^{-1}$  as followed from the DLS data. We have observed that the polymer dynamics qualitatively changes upon TNF addition, and these changes strongly depend on the polymer concentration and the acceptor content. We relate these changes to CTC formation in the MEH-PPV:TNF blends. Below we present the DLS data for four characteristic donor:acceptor blends: the dilute ( $C_D^0 = 0.5\text{ g l}^{-1}$ ) and the semidilute ( $C_D^0 = 2\text{ g l}^{-1}$ ) polymer solutions at low (1:0.5 and 1:0.05 for dilute and semidilute solutions, respectively) and at high (1:0.75 and 1:0.45 for dilute and semidilute solutions, respectively) acceptor content. These concentrations and donor:acceptor ratios are plotted in Fig. 1. As was found earlier,<sup>16</sup> the CTC concentration in the blend steeply increases at the threshold acceptor concentration  $C_A^c \sim 0.8\text{ g l}^{-1}$  (the dashed line in Fig. 1). The donor and acceptor concentrations for the characteristic blends were chosen so that  $C_A < C_A^c$  (low acceptor content) and  $C_A > C_A^c$  (high acceptor content).

### Low acceptor content

**Dilute solution.** Fig. 2 shows the DLS data for dilute pristine ( $0.5\text{ g l}^{-1}$ ) and blend (1:0.5) solutions. The strongest mode in the hydrodynamic radius distribution (HRD) of pristine MEH-PPV can be assigned to scattering from diffusing individual polymer coils.<sup>19</sup> Indeed, inset in Fig. 2b shows the

$q^2$ -dependence of the inverse relaxation time for the strongest mode: it is well fitted by the linear dependence  $\tau^{-1}(q^2) \sim Dq^2$  that indicates the diffusive motions of macromolecules with diffusivity  $D = (6.8 \pm 0.3) \times 10^{-8}\text{ cm}^2\text{ s}^{-1}$ . The hydrodynamic radius of the coils  $R_h = 35 \pm 5\text{ nm}$  was calculated from eqn (1). In the MEH-PPV HRD, a low-intensity mode is also observed at shorter relaxation times (Fig. 2b), which corresponds to scatterers of size  $\sim 6\text{ nm}$  according to eqn (1). This size could be assigned to the effective conjugated length of MEH-PPV that is about 4–7 nm.<sup>20,24</sup> The dilute solution ACF is extended to the long relaxation times upon TNF addition as follows from Fig. 1a. In the corresponding HRD, a slow mode appears in addition to the diffusion mode of isolated polymer coils (Fig. 2b). This slower mode corresponds to scatterers of a larger hydrodynamic radius ( $\sim 300\text{ nm}$ ) than that of the individual coils (eqn (1)). We assign the large scatterers to aggregates formed by polymer coils. The aggregates usually appear in the pristine polymer solution as a feature at long relaxation times upon increasing the polymer concentration above the overlap one.<sup>25</sup> In the corresponding ACF of  $1.5\text{ g l}^{-1}$  MEH-PPV solution an extended tail at long relaxation times is observed that is similar to the one observed in the donor–acceptor dilute blend (1:0.5) (see Fig. 1S in the ESI).<sup>†</sup> Although the polymer concentration in the blend is strongly decreased ( $\sim 0.4\text{ g l}^{-1}$ ) as compared with the pristine polymer (Fig. 1); however, the aggregates do appear in the blend. We conclude that TNF addition results in aggregation in the dilute blend. In the MEH-PPV:TNF solutions, the ground-state CTC is formed<sup>2–4</sup> so that the CTC can involve two conjugated segments with acceptor molecules being sandwiched between them.<sup>16</sup> One could suggest that the aggregates in the blend appear as a result of CTC formation involving *different* polymer coils as illustrated in Fig. 5a. Therefore, the CTC formation can induce interchain links resulting in macromolecule aggregates with an average hydrodynamic radius of  $R_A \sim 300\text{ nm}$ . We will refer to these aggregates as the *large* ones. Interestingly, the large aggregates live for several days and then disappear. That follows from the observation of the only band of diffusive polymer coils in the RTD. The disappearance of large aggregates could be explained with the domination of polymer–solvent interaction over the charge-transfer interaction involving different polymer

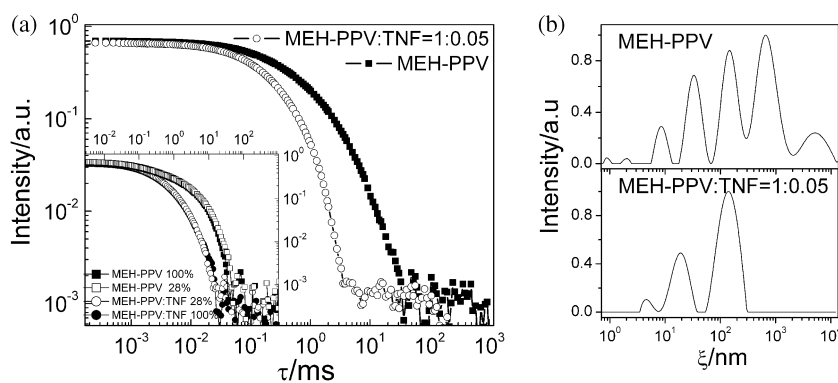


**Fig. 3** Semidilute solution data: (a) ACFs and (b) the corresponding CLDs for  $2\text{ g l}^{-1}$  pristine MEH-PPV solution (full squares) and for MEH-PPV:TNF = 1 : 0.05 (open circles) blend, the scattering vector  $q = 0.02\text{ nm}^{-1}$  ( $\theta = 90^\circ$ ). The inset in panel (a) shows the ACFs for different laser powers used for recording the DLS data.

chains. We conclude that in a dilute donor–acceptor blend with low acceptor content, TNF addition results in aggregates that disappear with solution aging. The CTC involving different polymer coils is suggested to be a cause of aggregation.

**Semidilute solution.** Fig. 3 displays ACFs (a) and the corresponding correlation length distributions (CLD) (b) for semidilute pristine ( $2 \text{ g l}^{-1}$ ) and blend ( $1:0.05$ ) solutions. The ACF for pristine MEH-PPV is extended to the long relaxation times that corresponds to the slow dynamics typical of semidilute solution,<sup>25–31</sup> and its CLD contains a series of closely located bands. The rich CLD spectrum in the pristine polymer corresponds to a variety of coupled motions of entangled chains in semidilute solution.<sup>25</sup> As Fig. 3a shows, the ACF narrows to the shorter relaxation times upon TNF addition, that is in contrast to the dilute solution. From comparison between the top and bottom graphs in Fig. 3b one can see that the number of bands in the CLD for the semidilute blend is decreased upon acceptor addition. Moreover, the bands at long correlation lengths disappear that is evidence of weakening the long-range correlations. We assign disappearing of the long-range correlations upon TNF addition to confinement of coupled motions of the entangled polymer chains. We suggest that such confinement stems from the CTC formation: a TNF molecule links two neighboring conjugated chains resulting in

a sandwich-like CTC.<sup>16,32</sup> As a result, these coupled segments could become constrained in their motion.

### High acceptor content

Fig. 4a and b show ACFs for the blends with high acceptor content in dilute and semidilute solutions, correspondingly. The pristine polymer ACFs are also shown for comparison. Fig. 4a and b indicate that the ACF shape in both blends depends on laser power. Note that, at low acceptor content, the ACFs in both blends do not depend on laser power (insets in Fig. 2a and 3a). As Fig. 4a–d show, at low power ( $\leq 9\%$  in the dilute solution and  $\leq 5\%$  in the semidilute one), the DLS data do not virtually depend on it. Therefore, one can conclude that, at low power, the DLS data give information about the dynamics of polymer chains. We relate the DLS data dependence on laser power to optical absorption in the blends at the excitation laser wavelength (633 nm). At high acceptor content, the optical absorption of MEH-PPV:TNF blends is much higher than that of the blends with low acceptor content.<sup>16</sup> This indicates that the power dependence results from high absorption in the blend. To probe the true macromolecule motion, we have to reduce the laser power until the ACF is independent of it.

**Dilute solution.** In the dilute solution at high acceptor content, the HRDs show the only diffusion band (Fig. 4c) with maximum at the hydrodynamic radius  $R_A \sim 100 \text{ nm}$

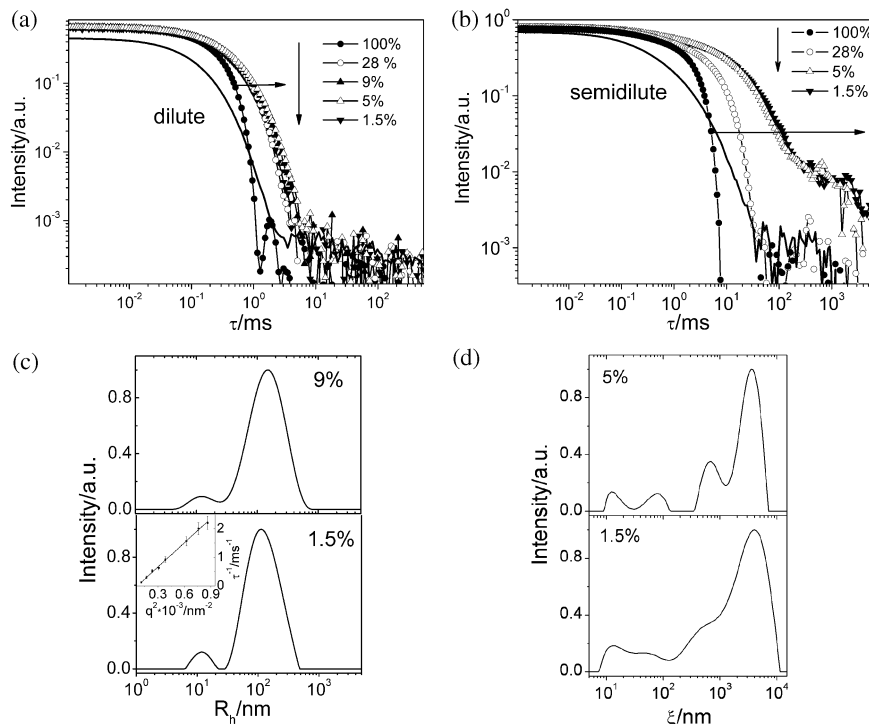


**Fig. 4** ACFs for MEH-PPV:TNF = 1:0.75 dilute ( $0.5 \text{ g l}^{-1}$ ) blend (a) and for MEH-PPV:TNF = 1:0.45 semidilute ( $2 \text{ g l}^{-1}$ ) blend (b) measured at different laser powers (the solid lines are the ACFs of pristine polymer solutions measured at 100% power) and the corresponding HRDs and CLDs for dilute (c) and semidilute (d) solutions, correspondingly. The inset in panel (c) shows the inverse relaxation time  $\tau^{-1}$  for dilute MEH-PPV:TNF = 1:0.75 dilute ( $0.5 \text{ g l}^{-1}$ ) blend vs. scattering vector, the line is a linear fit  $\tau^{-1} = Dq^2$  with  $D = (2.7 \pm 0.1) 10^{-8} \text{ cm}^2 \text{ s}^{-1}$ . The laser powers for HRDs and CLDs are listed in the upper corners. The scattering vectors were  $q = 0.02 \text{ nm}^{-1}$  ( $\theta = 90^\circ$ ) and  $q = 0.015 \text{ nm}^{-1}$  ( $\theta = 60^\circ$ ) for semidilute and dilute solutions, correspondingly.

(eqn (1)). Indeed, the linear dependence of the inverse relaxation time  $\tau^{-1}(q^2) \sim Dq^2$  is observed as shown in the inset, Fig. 4c. This diffusive motion could be assigned to polymer species with an increased radius as compared with the polymer coil radius in the dilute solution. One can calculate the radius of a sphere per polymer coil:

$$r_D = \sqrt[3]{\frac{3M_u N_u}{4\pi C_D \cdot N_A}}, \quad (2)$$

where  $N_u$  is the average number of monomers per coil,  $M_u$  is the monomer molecular weight, and  $N_A$  is the Avogadro number. Using the donor concentration  $C_D = 0.27 \text{ g l}^{-1}$  in the dilute blend MEH-PPV:TNF = 1:0.75 (see Fig. 1S),<sup>†</sup>  $M_u = 276.4$ , and  $N_u = 310$ ; we obtain  $r_D = 50 \text{ nm}$  that is two times less than the hydrodynamic radius of scatterers  $R_A \sim 100 \text{ nm}$ . Therefore, the MEH-PPV:TNF = 1:0.75 blend is expected to be semidilute. However, the observed ACF shape and the diffusion-type  $q^2$ -dependence of the characteristic decay indicate that the solution is dilute, with scatterers of hydrodynamic radius  $R_A \sim 100 \text{ nm}$  diffusing in it. Accordingly, we suggest that the band in Fig. 4c could be assigned to polymer aggregates. The hydrodynamic radius of these aggregates is three times smaller than that of the large aggregates, and we will refer to them as *small* aggregates. One could estimate the number of polymer coils in a small aggregate by using the condition of dilute solution. It means that the radius of a sphere per polymer aggregate must be larger than its radius  $r_D \geq R_A$ . Using eqn (2), one can estimate the number of coils per small aggregate:

$$N_c \geq \frac{4\pi C_D \cdot N_A \cdot R_A^3}{3 M_u N_u}, \quad (3)$$

that gives at least  $N_c \geq 7$  polymer coils involved into the small aggregates. Note that it is more correct to compare the theoretical value of  $r_D$  with the gyration radius of the scatterers. This radius could be obtained from the static light scattering studies; however, this is beyond the scope of the present paper. One can expect that the gyration radius of small aggregates is larger than the hydrodynamic one, as usually observed for polymer coils.<sup>18</sup> Therefore, one could suppose that  $R_A$  and  $N_c$  are the lower estimates of the aggregate radius and of the number of coils per aggregate, correspondingly.

The difference between the large and small aggregates observed, respectively, at low and high acceptor content in the dilute blends is as follows. First, the band of individual polymer coils at  $R_h \sim 35 \text{ nm}$  observed in the HRD at low acceptor content (large aggregates) is absent at high acceptor content (small aggregates). This implies that the majority of polymer coils are involved into the small aggregates in contrast to the large ones. Second, the small aggregates are much more stable than the large ones as the former do not disappear with aging the solution (several weeks), whereas the latter do. Therefore, in the dilute blend with high acceptor content, the interchain links mediated by CTCs are stronger than the polymer-solvent interaction. In contrast, at low acceptor content, the latter is dominated over the former. We assign the difference between the large and small aggregates to the different CTC concentration in the blends. As discussed above,

the CTC formation can involve different polymer chains resulting in interchain links and, hence, aggregation both at low and high acceptor content. However, at high acceptor content, the CTC concentration in MEH-PPV:TNF blends is more than 10 times higher than at low acceptor content.<sup>16</sup> It is natural to suppose that, at low acceptor content, there are much fewer CTCs that link different polymer coils to aggregates than those at high acceptor content. Therefore, the small aggregates are much more stable than the large ones as a result of much higher CTCs concentration. Briefly, in the dilute solution, the large aggregates with an average hydrodynamic radius  $R_A \sim 300 \text{ nm}$  and small ones with a radius  $R_A \sim 100 \text{ nm}$  appear at low and high acceptor content, correspondingly. The small aggregates are stable whereas the large ones are unstable, and this difference can be assigned to the difference in the concentration of CTCs forming the intercoil links.

**Semidilute solution.** In semidilute solution at high acceptor content, the ACFs and CLDs for the blend measured at low powers are peculiar to the coupled motion of entangled chains of a semidilute solution.<sup>25</sup> The ACF in pristine MEH-PPV solution falls to zero approximately at 30–50 ms, whereas the ACF in the blend with high acceptor content is extended to much longer relaxation times falling to zero at 5–7 s (Fig. 4b). The corresponding CLD (Fig. 4d) shows a dominant band at large correlation lengths 3–5  $\mu\text{m}$  (eqn (1)).

As follows from the Raman data, the CTC formation leads to planarization of the conjugated polymer segments involved in the CTC.<sup>15</sup> Indeed, the intensity of MEH-PPV Raman band at  $966 \text{ cm}^{-1}$  assigned to the out-of-plane CH bending vibration of the vinylene group decreases in the blend upon TNF addition.<sup>15</sup> This vibration is forbidden in the Raman spectrum for the planar configuration of the of oligo- and poly-paraphenylenevinylene chains.<sup>33</sup> Accordingly, the conjugated polymer segments become more planar upon CTC formation.<sup>15</sup> At high acceptor content, this planarization can stimulate further CTC formation as was earlier suggested.<sup>16</sup> One can suppose that aggregates of planarized conjugated segments linked by the CTCs are formed in semidilute solution at high acceptor content. We will refer to these aggregates as clusters. We assign the observed large-scale correlations ( $\sim 3\text{--}5 \mu\text{m}$ ) to their concentration fluctuations. In contrast, at low acceptor content, the CTC concentration is much lower;<sup>16</sup> therefore, the planarization of polymer conjugated segments appears to be insufficient to facilitate their intensive aggregation and cluster formation. This is suggested to result only in local confinement of entangled chain motion observed as the small-scale correlations ( $\sim 100 \text{ nm}$ ).

## Summary and conclusion

Fig. 5 summarizes the structural changes induced by CTC formation in all the characteristic MEH-PPV:TNF blends studied. The structural changes are suggested from the observed dominant relaxation modes with the use of the Einstein-Stokes relation. In dilute solution (Fig. 5a), the acceptor addition induces aggregation of polymer coils both at low and high acceptor content. At low acceptor content

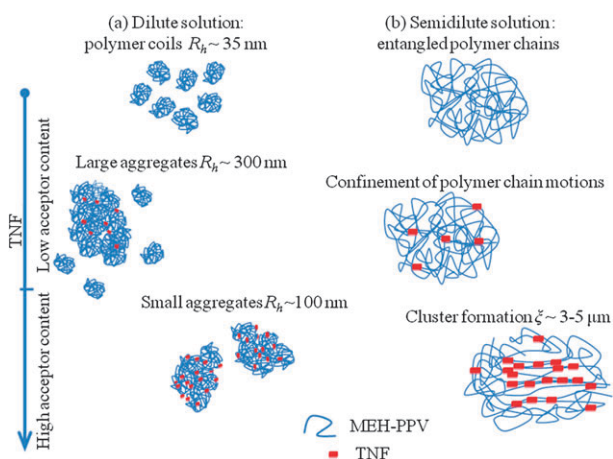


**Fig. 5** Illustration of the structural changes induced by CTC formation in dilute (a) and semidilute (b) blend solutions. The numbers are the hydrodynamic radii for the dilute solution and the correlation length for the semidilute one.

which corresponds to low CTC concentration, the aggregates are large ( $\sim 300$  nm) but not stable due to low concentration of the CTC links. At high acceptor content that corresponds to high CTC concentration, the aggregates are small ( $\sim 100$  nm) and stable due to high concentration of the CTC links. At high acceptor content, the majority of polymer chains are involved in the small aggregates, whereas at low acceptor content, only part of the chains are involved in the large aggregates. In semidilute solution (Fig. 5b), the changes in dynamics at low and high acceptor content are dramatically different. At low acceptor content, the low concentration of the CTC links does not change the conformational state of entangled polymer chains and leads only to confinement of their fluctuations so that small-scale correlations ( $\sim 100$  nm) are observed. At high acceptor content, a large amount of CTC links results in formation of clusters of planarized conjugated segments which results in large-scale correlations ( $\sim 3\text{--}5$   $\mu\text{m}$ ). Moreover, the conformational state of polymer chains also changes: a part of the chains becomes planarized which stimulates their aggregation into clusters.

The DLS technique has revealed the rich macromolecular dynamics of conjugated polymer blended with an organic acceptor. In a polymer blend with pronounced donor–acceptor charge-transfer interaction in the electronic ground state, the four distinct types of macromolecular dynamics have been observed depending on the polymer concentration and acceptor content. These new dynamics are assigned to the interchain links mediated by CTC formation (CTC links), with acceptor molecules being sandwiched between the polymer chains.

Thus, the DLS data clearly show that donor–acceptor blends of a conjugated polymer and an organic acceptor can be a far more complex system that could be anticipated from just a mixture of the two components. Importantly, the blend reveals new dynamic properties absent in the parent polymer. One can expect that the DLS technique could become a useful tool to study the nano- and microstructure of donor–acceptor conjugated polymer blends. Possibly, the donor–acceptor ground-state charge-transfer interaction could be used to influence and maybe even to control the blend film

morphology that can be inherited from the solution. This is of high importance for the development of efficient bulk heterojunctions for organic solar cells.

## Acknowledgements

We thank V. V. Bruevich and S. A. Zapunidi for fruitful discussions, M. Pshenichnikov and M. Bendikov for critical reading of the manuscript. This work was partially supported by the program “Scientific and scientific-educational personnel of innovative Russia” (contracts # 16.740.11.0064 and 16.740.11.0249).

## References

- 1 B. J. Schwartz, *Annu. Rev. Phys. Chem.*, 2003, **54**, 141.
- 2 D. Y. Parashchuk, S. G. Elizarov, A. N. Khodarev, A. N. Shchegolikhin, S. A. Arnautov and E. M. Nechvolodova, *JETP Lett.*, 2005, **81**, 467.
- 3 A. A. Bakulin, A. N. Khodarev, D. S. Martyanov, S. G. Elizarov, I. V. Golovnin, D. Y. Parashchuk, S. A. Arnautov and E. M. Nechvolodova, *Dokl. Chem.*, 2004, **398**, 204.
- 4 A. A. Bakulin, S. G. Elizarov, A. N. Khodarev, D. S. Martyanov, I. V. Golovnin, D. Y. Parashchuk, M. M. Triebel, I. V. Tolstov, E. L. Frankevich, S. A. Arnautov and E. M. Nechvolodova, *Synth. Met.*, 2004, **147**, 221.
- 5 L. Goris, K. Haenen, M. Nesladek, P. Wagner, D. Vanderzande, L. De Schepper, J. D’Haen, L. Lutsen and J. V. Manca, *J. Mater. Sci.*, 2005, **40**, 1413.
- 6 J. J. Benson-Smith, L. Goris, K. Vandewal, K. Haenen, J. V. Manca, D. Vanderzande, D. D. C. Bradley and J. Nelson, *Adv. Funct. Mater.*, 2007, **17**, 451.
- 7 A. A. Bakulin, D. S. Martyanov, D. Y. Parashchuk, M. S. Pshenichnikov and P. H. M. van Loosdrecht, *J. Phys. Chem. B*, 2008, **112**, 13730.
- 8 A. A. Bakulin, S. A. Zapunidi, M. S. Pshenichnikov, P. H. M. van Loosdrecht and D. Y. Parashchuk, *Phys. Chem. Chem. Phys.*, 2009, **11**, 7324.
- 9 A. A. Bakulin, D. Martyanov, D. Y. Parashchuk, P. H. M. van Loosdrecht and M. S. Pshenichnikov, *Chem. Phys. Lett.*, 2009, **482**, 99.
- 10 D. Veldman, O. Ipek, S. C. J. Meskers, J. Sweelssen, M. M. Koetse, S. C. Veenstra, J. M. Kroon, S. S. Van Bavel, J. Loos and R. A. J. Janssen, *J. Am. Chem. Soc.*, 2008, **130**, 7721.
- 11 K. Tvingstedt, K. Vandewal, A. Gadisa, F. Zhang, J. Manca and O. Inganäs, *J. Am. Chem. Soc.*, 2009, **131**, 11819.
- 12 K. Vandewal, K. Tvingstedt, A. Gadisa, O. Inganäs and J. V. Manca, *Nat. Mater.*, 2009, **8**, 904.
- 13 S. G. Elizarov, A. E. Ozimova, D. Y. Parashchuk, S. A. Arnautov and E. M. Nechvolodova, *Proc. SPIE*, 2006, **6257**, 293.
- 14 H. Hoppe and N. S. Sariciftci, *J. Mater. Chem.*, 2006, **16**, 45.
- 15 V. V. Bruevich, T. S. Makhmutov, S. G. Elizarov, E. M. Nechvolodova and D. Y. Parashchuk, *J. Chem. Phys.*, 2007, **127**, 104905/1.
- 16 O. D. Parashchuk, V. V. Bruevich and D. Y. Parashchuk, *Phys. Chem. Chem. Phys.*, 2010, **12**, 6021.
- 17 A. Yu. Grosberg and A. R. Khokhlov, *Statistical Physics of Macromolecules*, AIP Press, NY, 1994.
- 18 C. L. Gettinger, A. J. Heeger, J. M. Drake and D. J. Pine, *J. Chem. Phys.*, 1994, **101**, 1673.
- 19 T. Q. Nguyen, V. Doan and B. J. Schwartz, *J. Chem. Phys.*, 1999, **110**, 4068.
- 20 Y. C. Li, C. Y. Chen, Y. X. Chang, P. Y. Chuang, J. H. Chen, H. L. Chen, C. S. Hsu, V. A. Ivanov, P. G. Khalatur and S. A. Chen, *Langmuir*, 2009, **25**, 4668.
- 21 Y. C. Li, K. B. Chen, H. L. Chen, C. S. Hsu, C. S. Tsao, J. H. Chen and S. A. Chen, *Langmuir*, 2006, **22**, 11009.
- 22 P. S. Wang, H. H. Lu, C. Y. Liu and S. A. Chen, *Macromolecules*, 2008, **41**, 6500.
- 23 W. C. Ou-Yang, C. S. Chang, H. L. Chen, C. S. Tsao, K. Y. Peng, S. A. Chen and C. C. Han, *Phys. Rev. E*, 2005, **72**, 031802.

- 
- 24 T. P. Nguyen, V. H. Tran, P. Destruel and D. Oelkrug, *Synth. Met.*, 1999, **101**, 633.
- 25 W. Brown and T. Nicolai, *Colloid Polym. Sci.*, 1990, **268**, 977.
- 26 P. Stepanek and W. Brown, *Macromolecules*, 1998, **31**, 1889.
- 27 P. G. De Gennes, *Scaling Concepts in Polymer Physics*, Cornell University Press, Ithaca NY, 1979.
- 28 M. Adam and M. Delsanti, *Macromolecules*, 1985, **18**, 1760.
- 29 E. J. Amis and C. C. Han, *Polymer*, 1982, **23**, 1403.
- 30 Y. Einaga, A. Itaya and M. Takaoka, *Polymer*, 2002, **43**, 4869.
- 31 T. Norisuye, T. Morinaga, Q. Tran-Cong-Miyata, A. Goto, T. Fukuda and M. Shibayama, *Polymer*, 2005, **46**, 1982.
- 32 V. V. Bruevich, T. S. Makhmutov, S. G. Elizarov, E. M. Nechvolodova and D. Y. Paraschuk, *J. Exp. Theor. Phys.*, 2007, **105**, 469.
- 33 A. Sakamoto, Y. Furukawa and M. Tasumi, *J. Phys. Chem.*, 1992, **96**, 1490.